Fri. Feb. 09, 2018

- Reading:
  - Chapter 3 (Landsat)

- Today
  - Ch2. "Photographs" from Aircraft and Satellites
    - Note -- parts are "old" technology -- just look for principles, not details
      - Skip description of old imaging systems at the end.
      - Much better sources exist now -- will cover in Chapter 3
    - Stereo Imaging (review Wednesday lab)
      - Recent sources of data: NAPP (and older NHAP)
        - » http://glovis.usgs.gov/
    - Photomosaics
    - Phase angle, sun and vegetation effects

Using the Nomograph

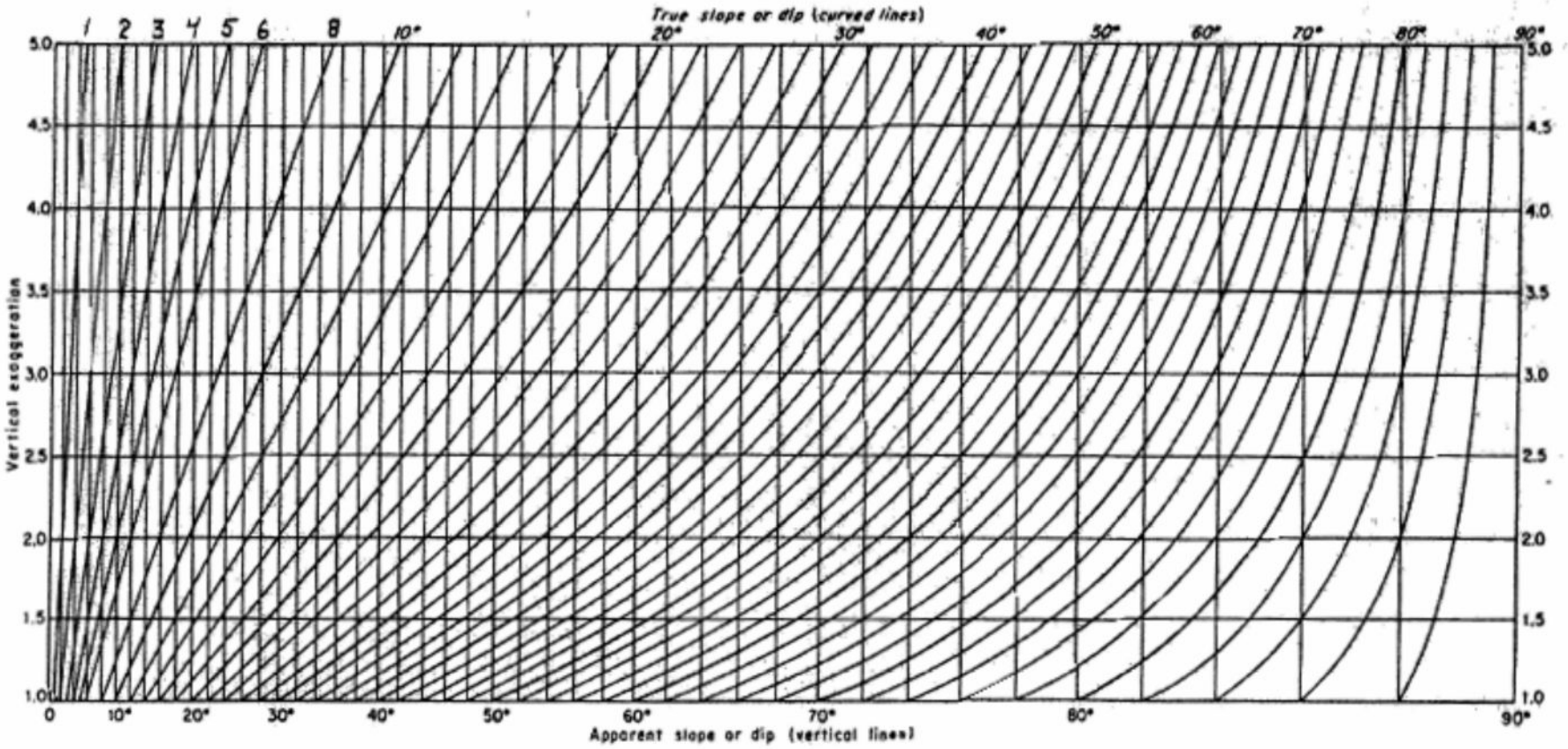

- Start with apparent slope at the bottom
- Move vertically upward to the correct vertical exaggeration
- Follow the curved line to the top of the plot where you then read the real slope

Aerial Photography Programs

- http://glovis.usgs.gov/
  - (aerial images removed from 2018 version)
- http://earthexplorer.usgs.gov/

- NHAP (National High Altitude Photograph) program 1980-1989
- NAPP (National Aerial Photography Program)
  1987-2007, repeat coverage every 5-7 years
  Online images have pixel size of ~2.5 meters

- Since then -- USGS buying special purpose commercial coverage of limited regions (satellite, aircraft)

- Repeat satellite coverage available from Landsat, and other satellites we'll discuss later.

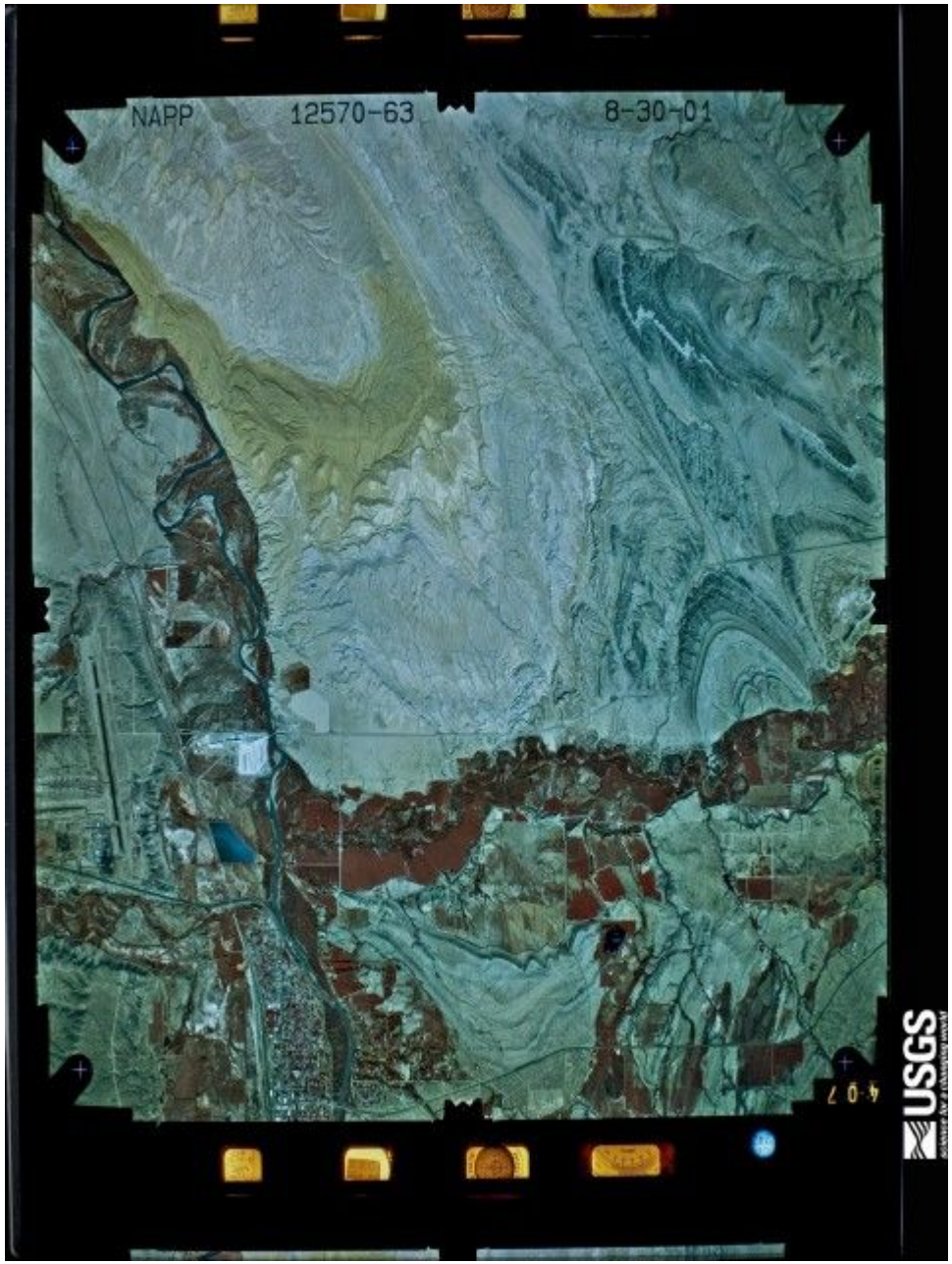

NAPP
Color IR (False Color)
Greybull, WY
Sheep Mountain

- http://glovis.usgs.gov/

NAPP
Alkali Anticline
Bighorn Basin

- http://glovis.usgs.gov/
- Laramie example on-line
  - Lat, Long = 41.3 -105.6

NAPP
Alkali Anticline
Bighorn Basin

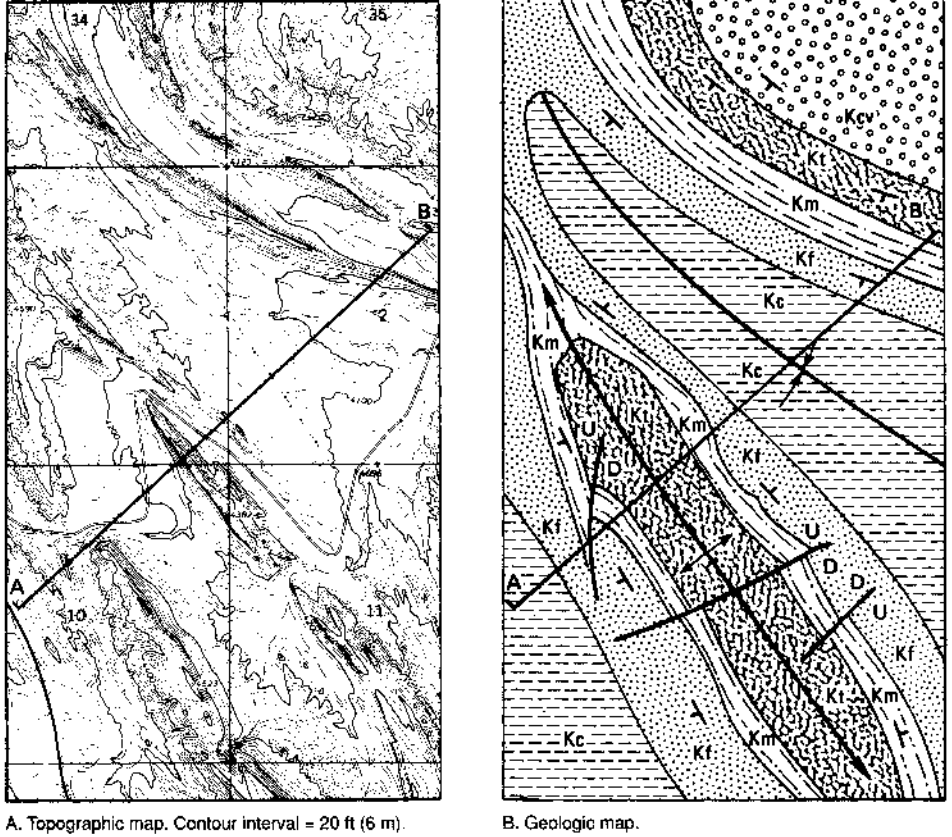

A. Topographic map. Contour interval = 20 ft (6 m).

B. Geologic map.

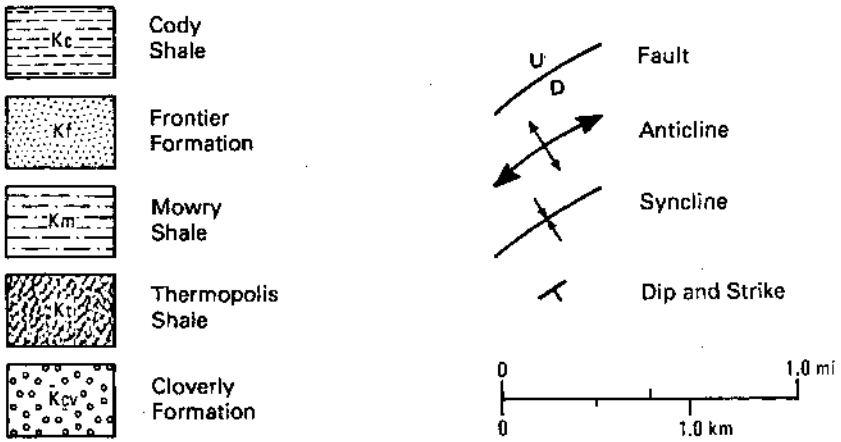

C. Formation symbols.

D. Structure symbols.

Figure 2-14 Topographic and geologic maps of the Alkali anticline, Bighorn Basin, Wyoming.

- Lab 2 (and 3 maps) should be similar to this (except use colored lines, rather than stippling, etc.

Online glovis demonstration

- http://glovis.usgs.gov/
  - Aerial images seemed to have been removed in 2018 version -- use Earth Explorer for those.
  - Laramie example on-line
    - Lat, Long = 41.3 -105.6
- http://earthexplorer.usgs.gov/

Io Stereo

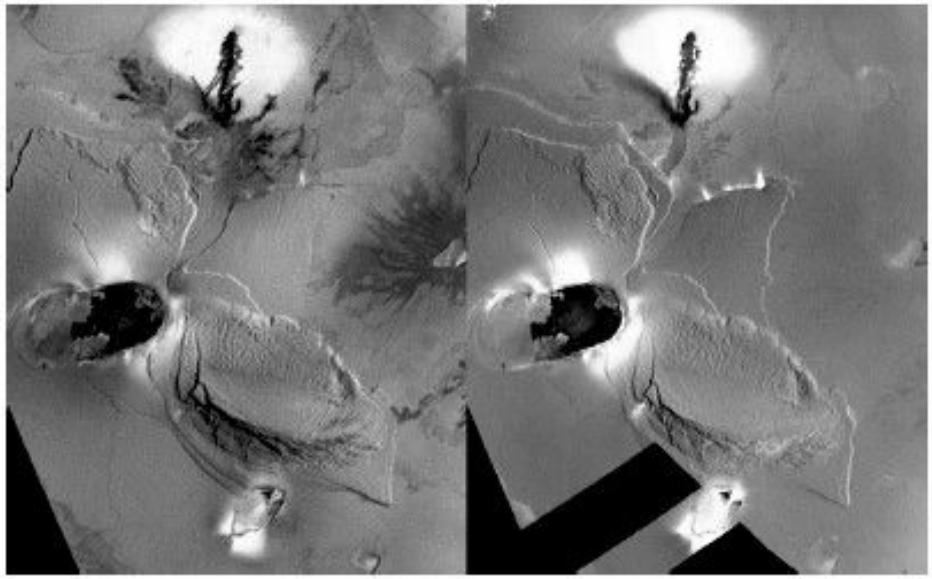

Fig. 1. Stereoimage pair of Euboea Montes, Io, obtained from Voyager 1 in 1979. Euboea Montes is the large massif near image center; Creidne Patera is the oval caldera with dark lava flows at center left adjacent to Euboea Montes. Voyager images FDS 16390.38 (right) and 16392.59 (left) are shown. Stereopair has a convergence angle of 49° and a base-to-height ratio of 1.5. Scene width is ~550 km. See Fig. 2 for north orientation and scale.

- Computer generated elevations based on measured shifts within digital stereo pairs

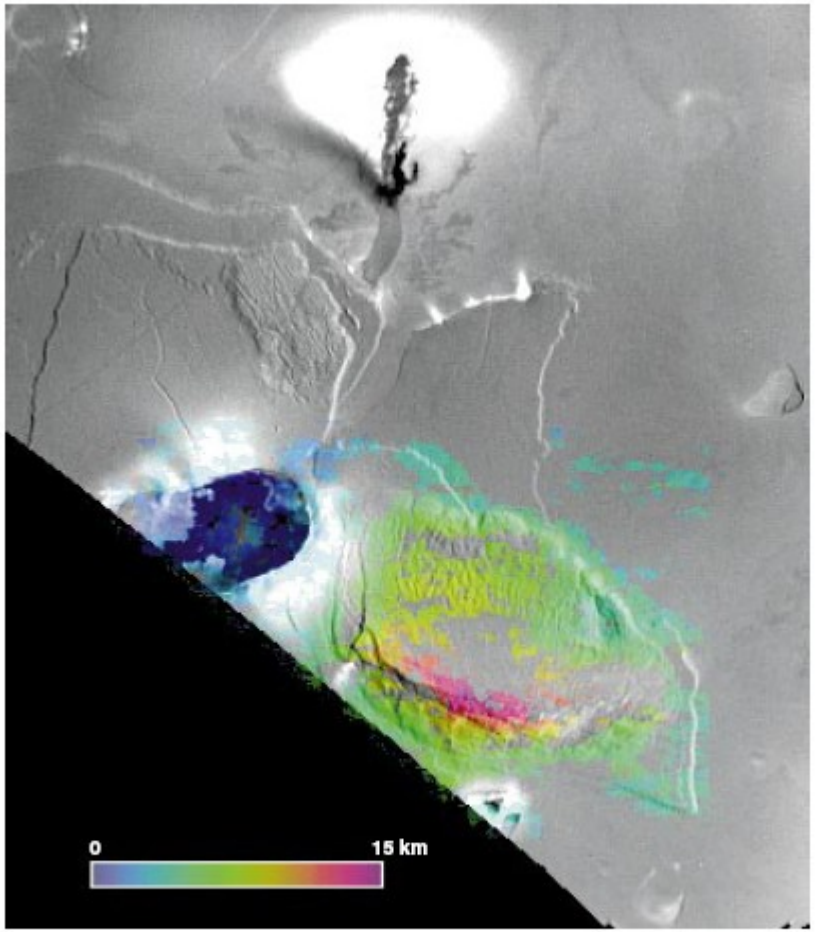

Fig. 3. Color-coded topographic map of Euboea Montes, derived from digital stereogrammetry (5). Color scale bar indicates relative elevations. Gaps in the data (uncolored areas) are where the stereogrammetric software failed to obtain a solution because of lack of detail or anomalous brightness patterns (5), or where data were not sampled. Image location and map scale correspond to Figs. 1 and 2.

Schenk et al. 1998

Photomosaics

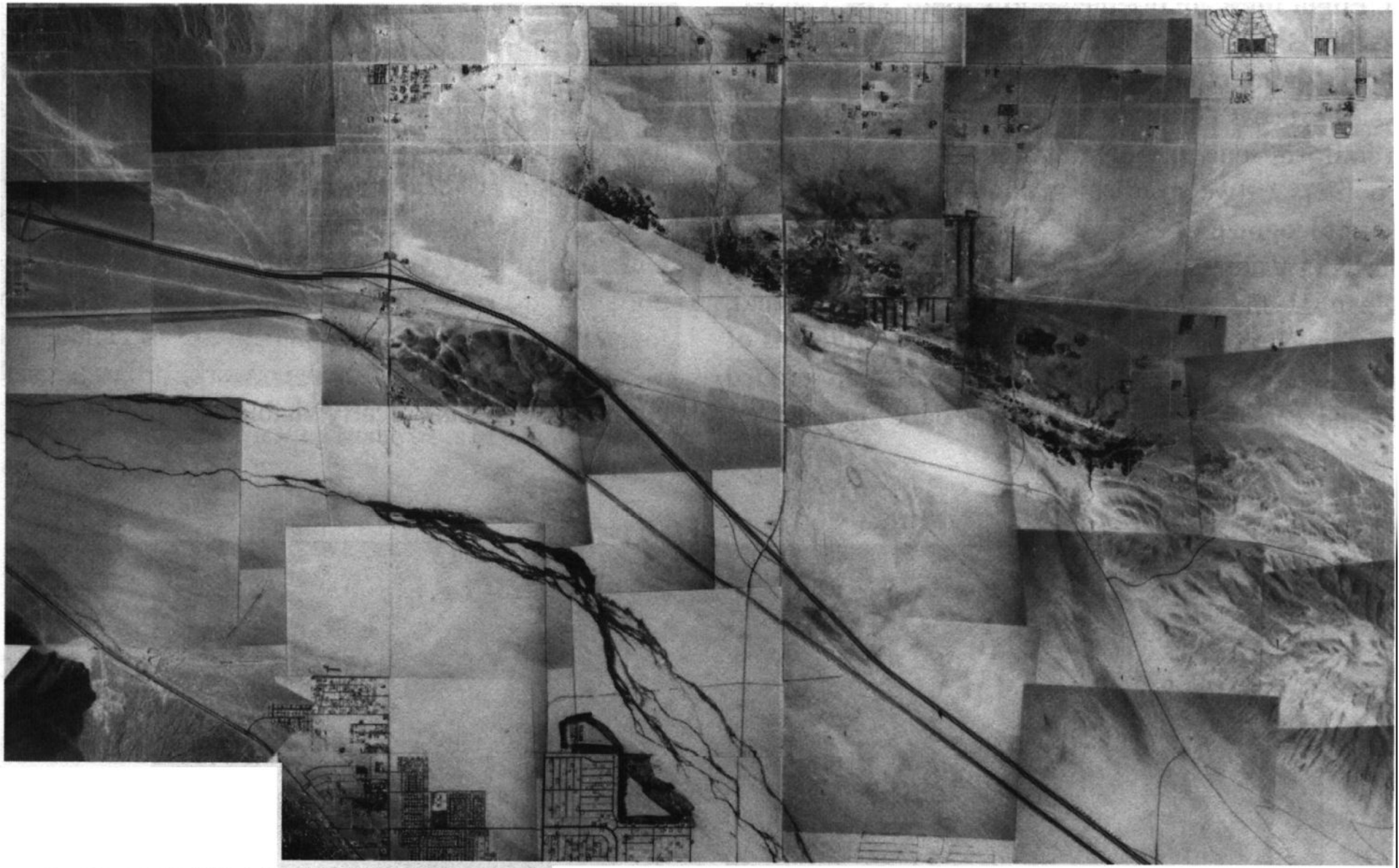

A. Photomosaic. From Sabins (1973A, Figure 6).

- Fig. 2-10: Coachella Valley, CA

Photomosaics

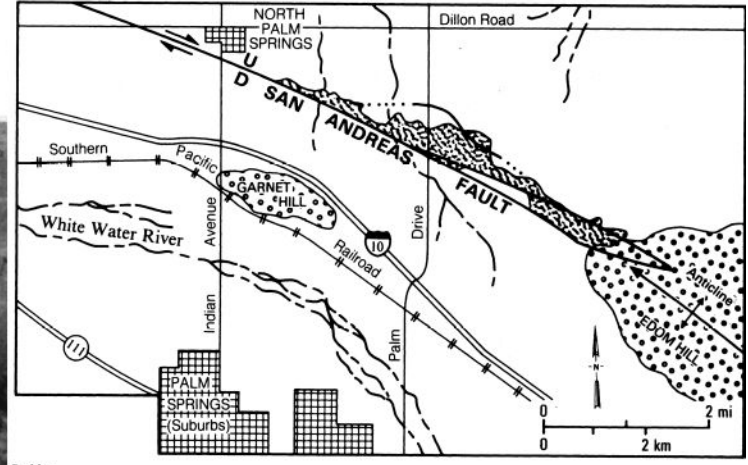

Figure 2-10 Photomosaic and map of Coachella Valley, California.

A. Photomosaic. From Sabins (1973A, Figure 6).

- Fig. 2-10: Coachella Valley, CA

Modern (Io/Galileo) Photomosaics

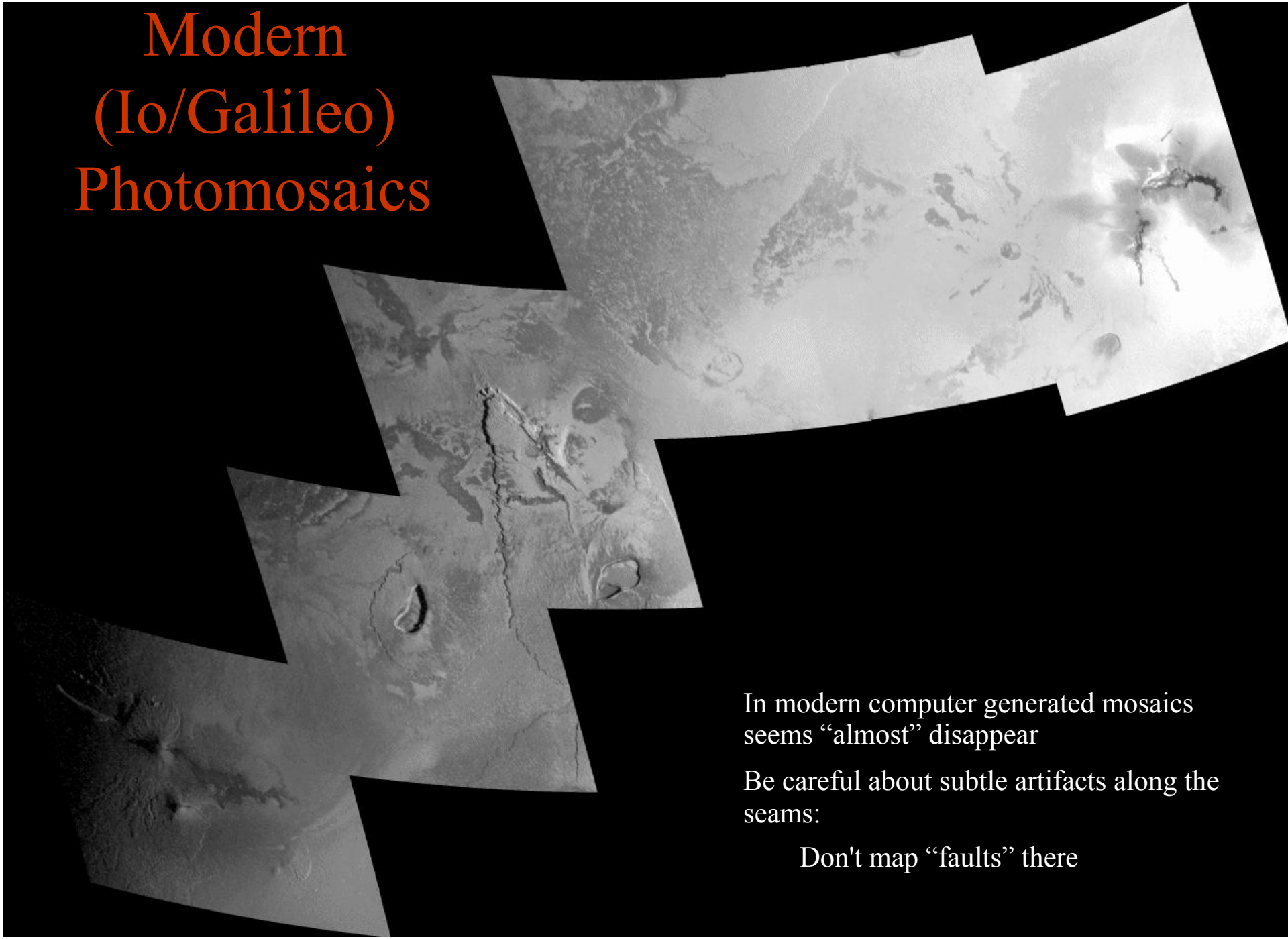

In modern computer generated mosaics seems “almost” disappear

Be careful about subtle artifacts along the seams:

- Don't map “faults” there

Effects of Sun Angle on Lunar Photos

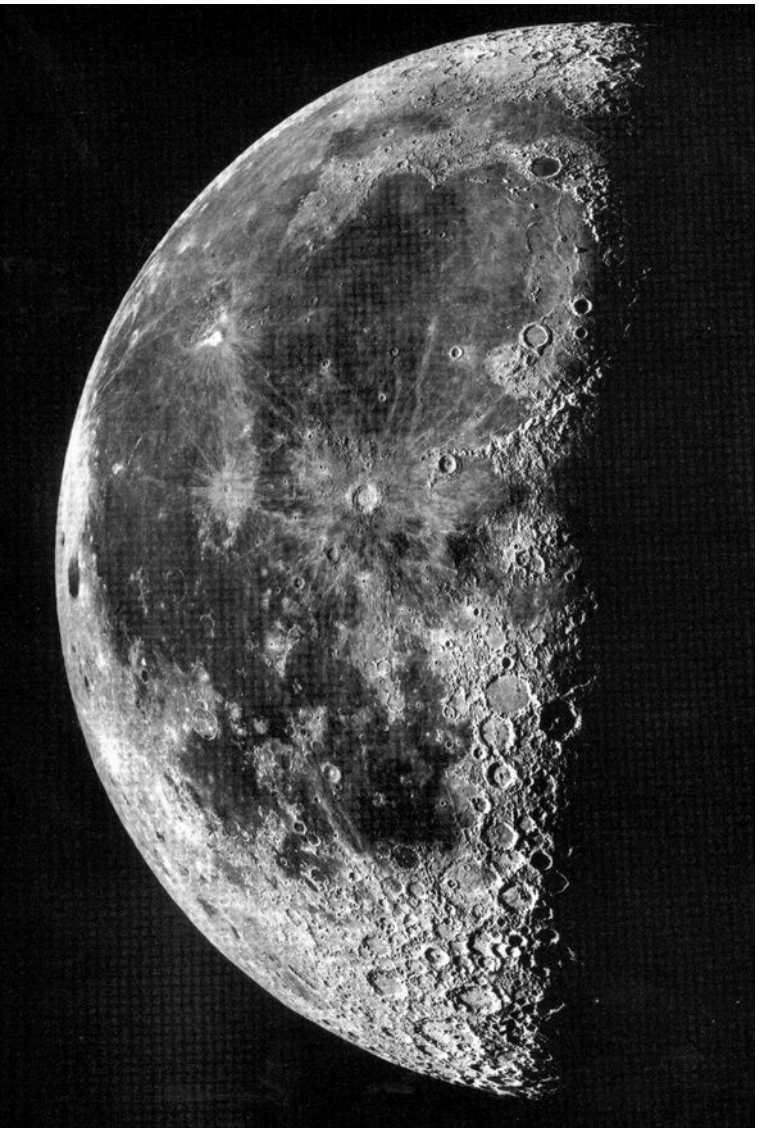

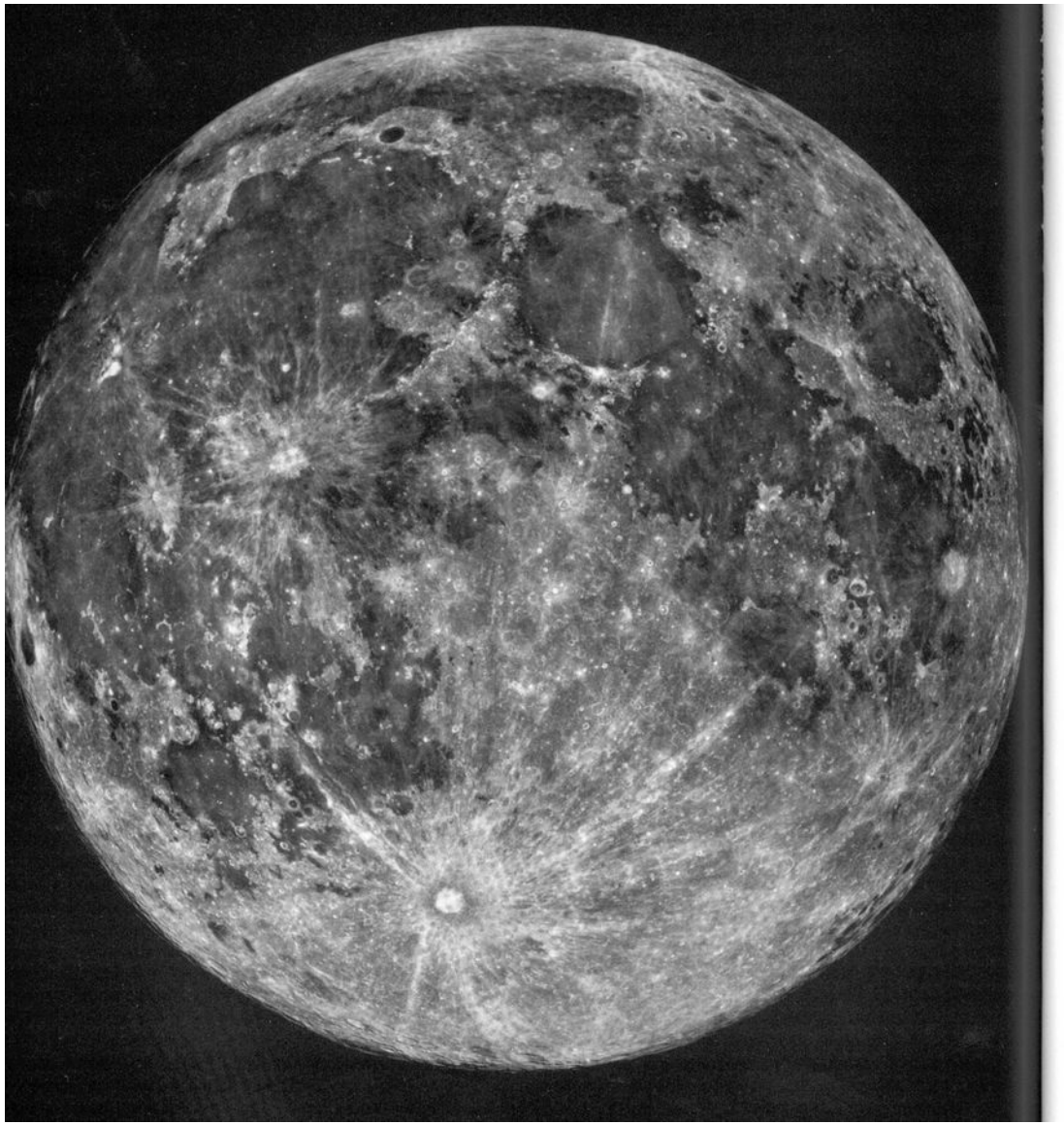

Sabins Sun Angle Effects

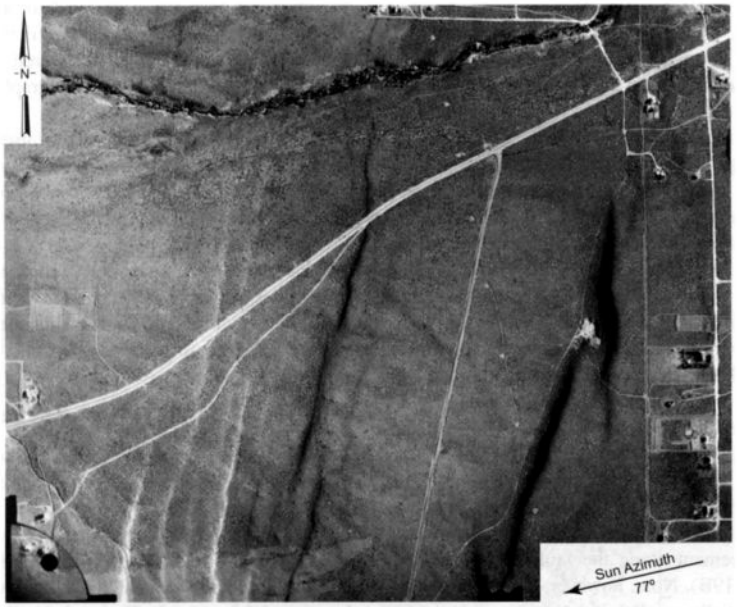

A. Low-sun-angle photograph acquired June 23, 1972, at 5:30 a.m. local sun time with sun elevation of 15°. From Walker and Trexler (1977, Figure 3).

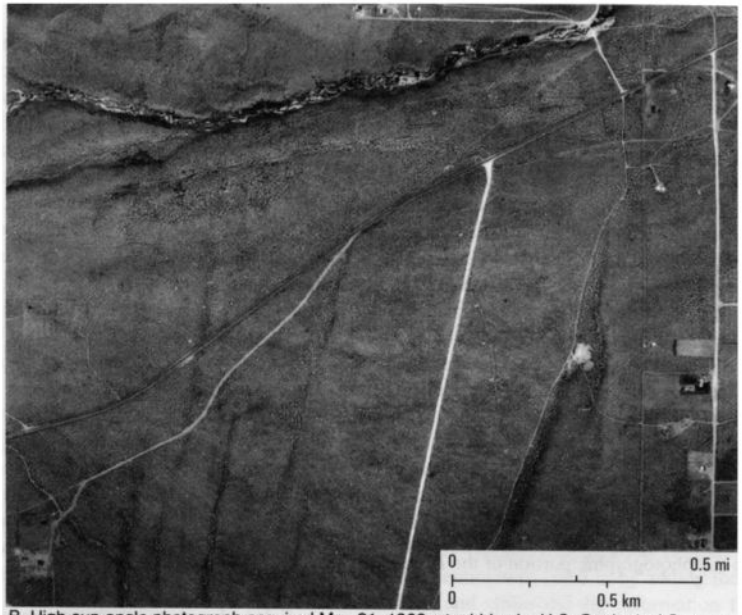

B. High-sun-angle photograph acquired May 21, 1966, at midday by U.S. Geological Survey.

Figure 2-18 Low-sun-angle photograph and high-sun-angle photograph of east flank of Carson Range, Nevada.

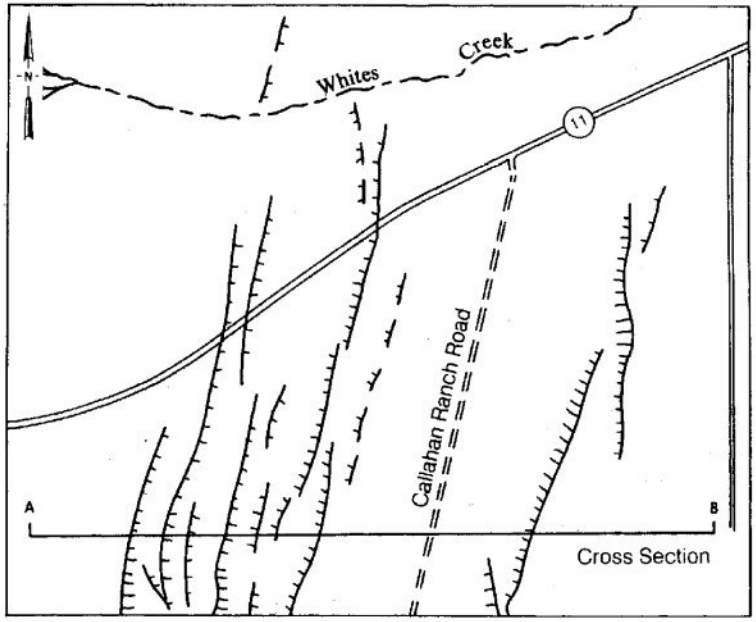

A. Interpretation map.

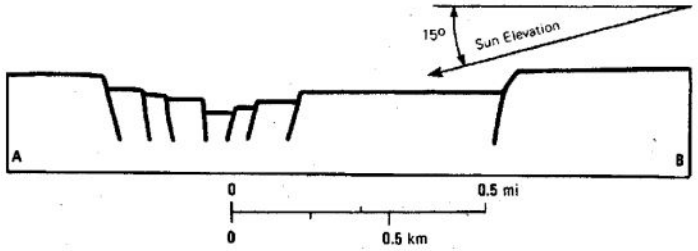

B. Vertically exaggerated cross section along line AB.

Figure 2-19 Interpretation map and cross section of the low-sun-angle photograph in Figure 2-18A.

- Scarps more evident in "low sun angle" image

Effect of snow, plus sun angle

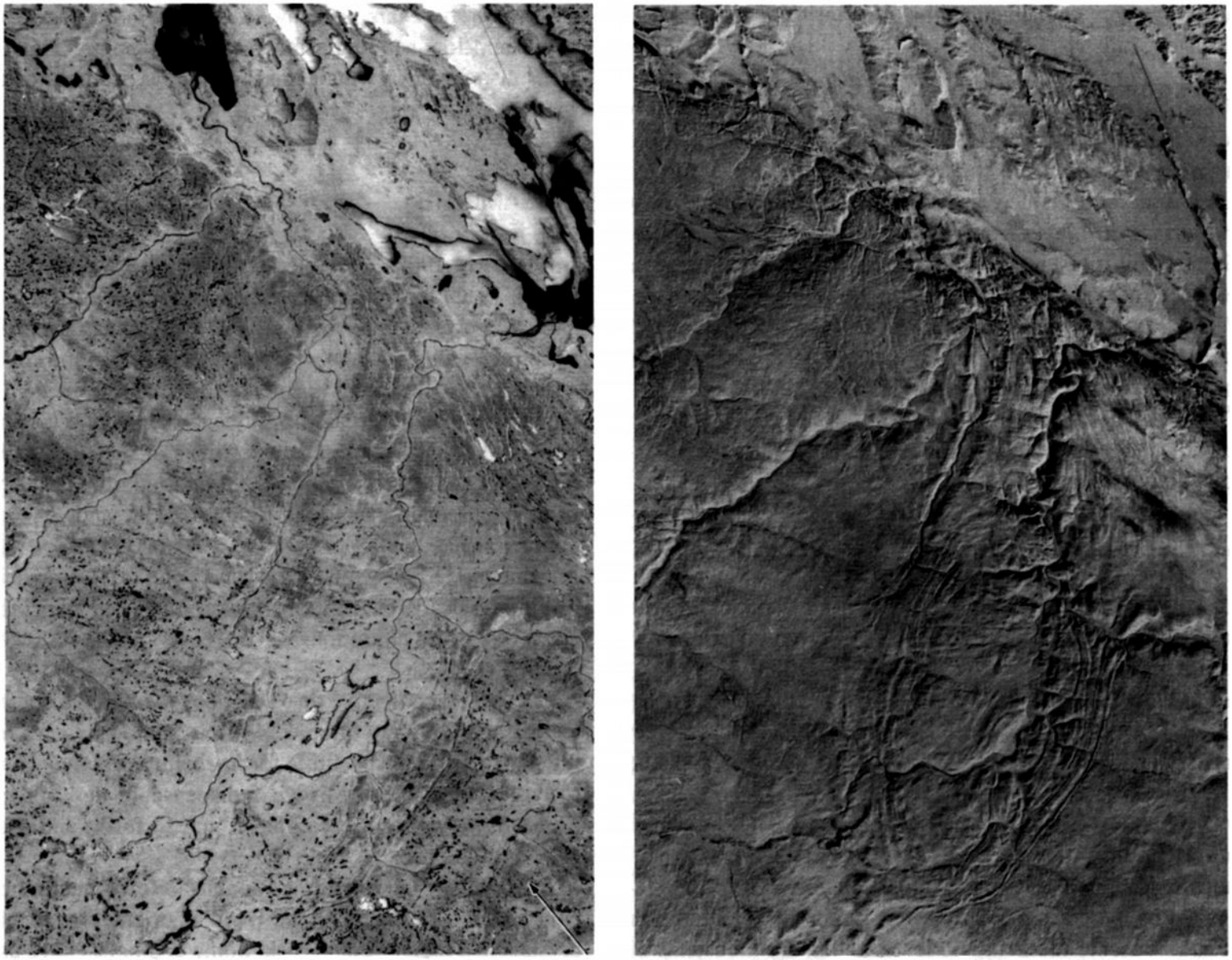

A. Summer image acquired June 18, 1973, with a 45° sun elevation.

B. Winter image acquired April 2, 1974, with a 27° sun elevation.

Sabins Fig. 3-22

Figure 3-22 Landsat MSS band 4 seasonal images of Bathurst Inlet, Arctic Canada.

Vegetation Effects

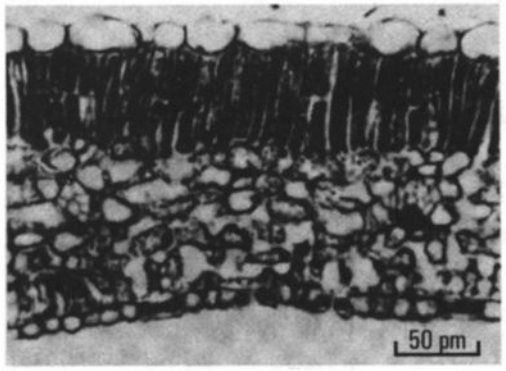

A. Nonstressed.

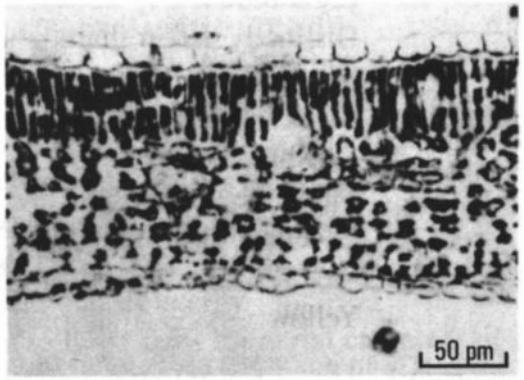

B. Stressed.

Figure 2-29 Photomicrographs of cross sections of nonstressed and stressed leaves. Collapse of cells in the mesophyll layer strongly reduces reflectance of incident IR energy. From Everitt and Nixon (1986, Figure 1). Courtesy J. H. Everitt, U.S. Department of Agriculture.

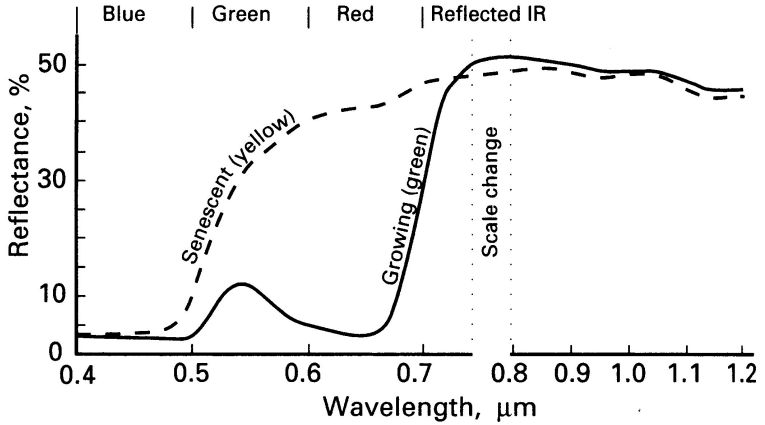

Figure 2-30 Reflectance spectra of green and senescent foliage. In the autumn, chlorophyll deteriorates, which reduces the absorption of incident red energy. The development of anthocyanin and tannin causes the yellow-red fall colors. From Schwaller and Tkach (1985, Figure 2).

- Conifers usually have lower reflectance in near-IR than deciduous trees
- Much of near-IR light scattered from leaves scatters off the interior structures, not just the leaf surface
- Changes in water content/stress of leaves changes amount of reflected IR
- As growing season ends chlorophyll disappears, red reflectance goes up
  - First symptom is often a shift in the λ of the red absorption edge

Figures from our text by Sabins